Mesoporous Metal–Metalloid Amorphous Alloys: The First Synthesis of Open 3D Mesoporous Ni-B Amorphous Alloy Spheres via a Dual Chemical Reduction Method

Yunqing Kang, Joel Henzie, Huajun Gu, Jongbeom Na, Amanullah Fatehmulla, Belqes Saeed A. Shamsan, Abdullah M. Aldhafiri, W. Aslam Farooq, Yoshio Bando, Toru Asahi, Bo Jiang,* Hexing Li,* and Yusuke Yamauchi*

Selective hydrogenation of nitriles is an industrially relevant synthetic route for the preparation of primary amines. Amorphous metal–boron alloys have a tunable, glass-like structure that generates a high concentration of unsaturated metal surface atoms that serve as active sites in hydrogenation reactions. Here, a method to create nanoparticles composed of mesoporous 3D networks of amorphous nickel–boron (Ni-B) alloy is reported. The hydrogenation of benzyl cyanide to β-phenylethylamine is used as a model reaction to assess catalytic performance. The mesoporous Ni-B alloy spheres have a turnover frequency value of 11.6 h^{-1}, which outperforms non-porous Ni-B spheres with the same composition. The bottom-up synthesis of mesoporous transition metal–metalloid alloys expands the possible reactions that these metal architectures can perform while simultaneously incorporating more Earth-abundant catalysts.

1. Introduction

Amorphous metal alloys, or glassy metals, have unusual physical and chemical properties that stem from their lack of long-range crystallographic order.[1,2] They have long been identified as good heterogeneous catalysts,[3] and perform well in hydrogenation reactions.[4–6] The interaction between the metal–metalloid components in amorphous metals generates an electronic structure that is significantly different from its crystalline counterparts. The inclusion of the metalloid affects the local bond structure of the metal and creates a high concentration of unsaturated surface atoms.[7] Nickel–boron (Ni-B), in particular, is a promising catalyst because both elements are relatively inexpensive and Earth-abundant, thus it has attracted a lot of interest because it can hydrogenate various kinds of unsaturated bonds, including alkenes (C=C), aldehydes (HC=O), and nitriles (C≡N).[8–11] The morphology of heterogeneous catalysts impacts their properties and drives their activity and selectivity in catalytic reactions.[12] Presently, most work on Ni-B catalysts has focused on

Y. Kang, H. Gu, Prof. H. Li
The Education Ministry Key Lab of Resource Chemistry and Shanghai
Key Laboratory of Rare Earth Functional Materials
Shanghai Normal University
Shanghai 200234, China
E-mail: hexing-li@shnu.edu.cn

Y. Kang, Dr. J. Henzie, Dr. J. Na, Prof. Y. Bando, Dr. B. Jiang,
Prof. Y. Yamauchi
International Center for Materials Nanoarchitectonics (WPI-MANA)
National Institute for Materials Science (NIMS)
1-1 Namiki, Tsukuba, Ibaraki 305-0044, Japan
E-mail: jiang.bo@nims.go.jp; y.yamauchi@uq.edu.au

Y. Kang, Prof. T. Asahi
Faculty of Science and Engineering
Waseda University
3-4-1 Okubo, Shinjuku, Tokyo 169–8555, Japan

Dr. J. Na, Prof. Y. Yamauchi
School of Chemical Engineering and Australian Institute for
Bioengineering and Nanotechnology (AIBN)
The University of Queensland
Brisbane, QLD 4072, Australia

Prof. A. Fatehmulla, B. S. A. Shamsan, Prof. A. M. Aldhafiri,
Prof. W. A. Farooq
Department of Physics and Astronomy
College of Science
King Saud University
P.O. Box 2455, 11451 Riyadh, Saudi Arabia

Prof. Y. Bando
Institute of Molecular Plus
Tianjin University
No. 11 Building, No. 92 Weijin Road, Nankai District
Tianjin 300072, P. R. China

Prof. Y. Bando
Australian Institute for Innovative Materials (AIIM)
University of Wollongong
Squires Way, North Wollongong, NSW 2500, Australia

Prof. H. Li
Shanghai University of Electric Power
Shanghai 200062, China

Prof. Y. Yamauchi
Department of Plant & Environmental New Resources
Kyung Hee University
1732 Deogyeong-daero, Giheung-gu, Yongin-si
Gyeonggi-do 446–701, Republic of Korea

ADVANCED
SCIENCE NEWS
www.advancedsciencenews.com

NANO · MICRO

small
www.small-journal.com

nanoparticle morphologies.[13–16] In this paper, we shift this attention to examine the catalytic performance of mesoporous structures[17–22] with high surface areas, adjustable pore sizes, and narrow pore-size distributions.

We previously described a method to generate mesoporous metal nanoparticles using soft polymeric micelle templates that control the reduction of metal ions and make mesoporous metal nanoparticles,[17,21,22] but these templating methods are challenging for Ni because its reduction potential is very low (Ni^{2+}/Ni: −0.257 V vs SHE) compared to noble metal ions (e.g., Pt^{2+}/Pt: + 1.188 vs SHE). Thus, it is hard to reduce Ni ions with more gentle reducing agents such as ascorbic acid or formic acid. Some efforts in this field have been tried to obtain Ni-B mesoporous amorphous alloys via stronger reducing agent borohydrides ($NaBH_4$, KBH_4) and/or dimethylamine borane (DMAB), which also serve as boron sources.[23–26] For example, Li et al.[23] synthesized mesoporous amorphous Ni-B hydrogenation catalysts via the self-assembly of hexadecyltrimethylammonium bromide (CTAB) surfactants, and an electroless deposition method described by Yamauchi et al.[25,26] was used to obtain highly ordered mesostructured Ni-B materials. Unfortunately, the mesoporous Ni-B prepared by these two methods generate worm-like pores[23,24] or 2D straight-channel nanospheres filled with surfactants.[25,26] 3D porous materials are a good morphology for catalysis because open networks expose more active sites and have low tortuosity, which enhances mass transport.[27–29]

Amines are important intermediates in the synthesis of many compounds and fine chemicals. Catalytic hydrogenation of nitriles with hydrogen and catalysts is a practical, green, and atom-economical method for the synthesis of primary amines.[30,31] However, obtaining good selectivity is challenging because nitriles are readily hydrogenated to secondary and tertiary amines.[32,33] Past reports show that homogeneous catalysts are most successful in obtaining high selectivity for primary amines,[30,34] but applications of conventional homogenous catalysts are limited by the difficulty to collect/recover them after the reaction. Hence, heterogeneous non-noble metal catalysts tend to be more desirable when economics is a concern. In this study, we designed a method to synthesize nanoparticles composed of open 3D networks of mesoporous Ni-B amorphous alloy spheres. Uniformly sized spherical micelles made of diblock copolymer, poly(ethylene oxide)-*b*-poly (methyl methacrylate) (PEO-*b*-PMMA), serve as the pore-directing agent and sacrificial template. Inclusion of mesopores in Ni-B boosts the catalytic performance of the alloyed material in the hydrogenation of benzyl cyanide (BC) to *β*-phenylethylamine (*β*-PEA).

2. Results and Discussion

Scheme 1 illustrates the synthetic method used to generate mesoporous Ni-B amorphous alloy spheres. Additional details are located in Section 4. The synthetic procedure uses the self-assembly of surfactants and follows these steps: 1) A water–DMF mixture induces the micellization of PEO-*b*-PMMA, forming a core–shell structure composed of a PMMA core and PEO shell. 2) The PEO shell interacts with the metal Ni^{2+} cations via hydrogen bonds. 3) The addition of trace initiator SBH drives nucleation followed by particle growth via DMAB, and 4) the micelle template is removed with acetone, revealing mesoporous Ni-B amorphous alloy spheres. Figure S1a–c, Supporting Information, shows the formation of micelles, which illustrates the Tyndall effect upon mixing of the solvents. A negative staining technique using phosphotungstic acid (PW) shows that the average diameter of the PMMA micelles is ≈14.8 nm in TEM (Figure S1d, Supporting Information).[35,36] The process diagram of the reduction reaction is shown in Figure S2, Supporting Information. DMAB is a weaker
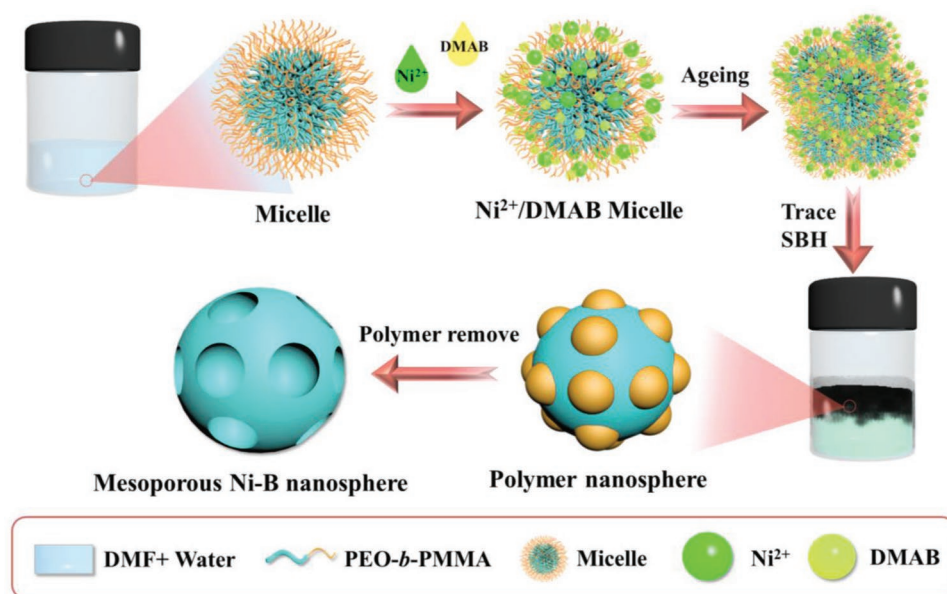
Scheme 1. Scheme for the preparation of the open 3D mesoporous Ni-B amorphous alloy spheres.
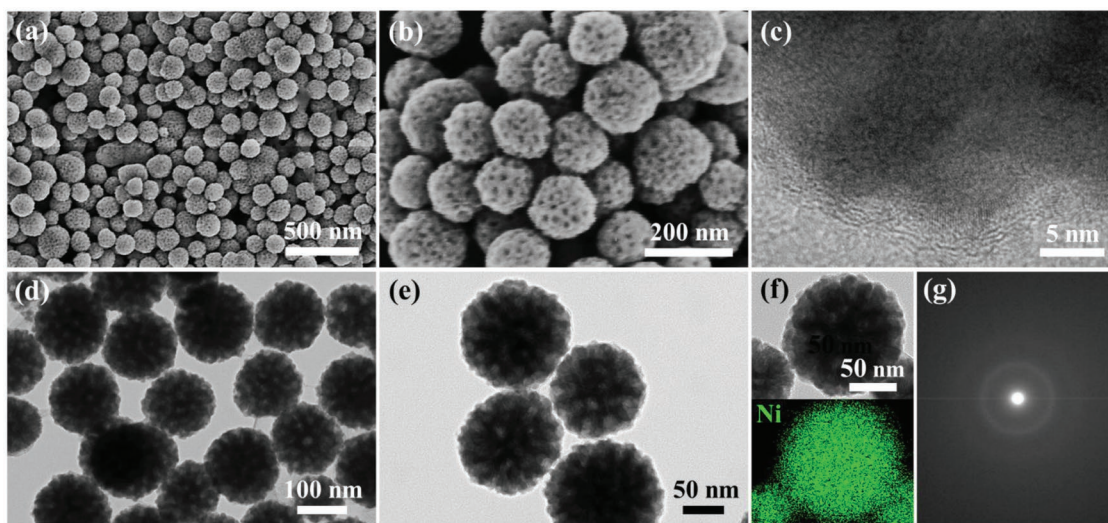
Figure 1. Structural characterization of the open 3D mesoporous Ni-B amorphous alloy spheres. a) Low-magnification and b) high-magnification SEM micrographs; scale bar: a) 500 nm, b) 200 nm. c–e) TEM images at different magnifications, and f) TEM image and corresponding Ni mapping. g) SAED pattern of a single mesoporous Ni-B alloy sphere. In Figure (c), the fringes on the edges are primarily carbon generated during the TEM observation. Some fringes of small Ni-B domains can be confirmed at the interior of the particle.

reducing agent than SBH and is stable at the reaction temperature. For example, the reduction process cannot be triggered without SBH, nor can it proceed beyond the nucleation process without DMAB (Figure S3, Supporting Information). When SBH is used exclusively as the reducing agent, the reaction proceeds too quickly to generate the mesoporous structure and can generate only agglomerated ultrafine Ni-B nanospheres, even at low temperatures (Figure S4, Supporting Information). Thus, this two-component SBH/DMAB reducing agent system is essential to forming the mesoporous network.

Figure 1 shows the scanning electron microscopy (SEM) and transmission electron microscopy (TEM) images of the open 3D mesoporous Ni-B nanostructures after the removal of the polymer template. Large-sized ≈14 nm diameter pores can be seen perforating the entire outer surface of the Ni–B nanospheres (Figure 1a,b). The average diameter of the mesoporous Ni–B spheres is ≈142 nm which was obtained by measuring >200 spheres (Figure S5, Supporting Information). It is challenging to generate a uniform distribution of the nuclei with SBH, but SBH is necessary to initiate the particle growth phase with DMAB. The long duration of the growth phase may also lead to some polydispersity. The porous structure can be observed in the TEM images (Figure 1d,e), while the Ni-B alloy sample prepared by omitting polymer micelles from the standard reaction shows a non-porous spherical shape with an average diameter of ≈333 nm (i.e., non-porous Ni-B alloy spheres) (Figure S6, Supporting Information). The block copolymer micelles serve as a template to generate pores in the metal. The selected-area electron diffraction (SAED) pattern (Figure 1g) confirms that the mesoporous Ni-B spheres are amorphous. Energy-dispersive X-ray spectroscopy (EDS) image shows that Ni is homogeneously distributed throughout the particle, while the boron is too light to observe (Figure 1f). The HRTEM (Figure 1c) indicates that there is no noticeable long-range atomic alignment because there are few clear domains

with lattice fringes.[37] ICP analysis indicates that the B content is ≈14 at% (Table S1, Supporting Information).

The wide-angle X-ray diffraction (XRD) was used to determine the amorphous structure of the synthesized mesoporous Ni-B alloy spheres (**Figure 2**a). There are no visible diffraction peaks for both mesoporous Ni-B and non-porous Ni-B, except for a weak broad peak located at $2\theta = 45°$, matching the typical amorphous XRD pattern for this material.[38] The small-angle X-ray scattering (SAXS, Figure 2b) was used to determine the periodicity of the mesoporous structure of mesoporous Ni-B. It has a broad peak located at $q = 0.25$ nm^{-1}, which indicates that the spherical pores are packed tightly together. The pore-to-pore distance is ≈25 nm, matching the measured SEM image (Figure S7, Supporting Information). The N$_2$ adsorption-desorption isotherm (Figure 2c) with a hysteresis is indicative of mesoporous structures.[39] Figure S8, Supporting Information, shows the N$_2$ adsorption–desorption isotherm of non-porous Ni–B. The data of Brunauer–Emmett–Teller (BET) surface area (S_{BET}) and the pore volume (V_{Pore}) obtained from N$_2$ isotherms are listed in Table S1, Supporting Information. The mesoporous Ni-B amorphous alloy spheres have a much larger S_{BET} (102.5 m^2 g^{-1}) than the non-porous Ni-B (12.0 m^2 g^{-1}), which could contribute to a higher catalytic activity.

EXAFS was used to examine the local structure of the as-prepared mesoporous Ni-B amorphous alloy spheres.[40] The radial distribution function (RDF) curve of the samples was obtained from their $\chi(k)k^3$ via a Fourier transform (Figure 2d). Ni foil reference material has distinct first, second, and third nearest-neighbor peaks because it has long-range order. We observe one broad peak for both mesoporous Ni-B and non-porous Ni-B samples, indicating that ordering is limited to first-nearest-neighbor structure and an overall lack of crystallinity.[41] The positions of the first coordination peak for amorphous Ni-B and Ni foil are 2.09 and 2.16 Å, respectively (Figure 2d).
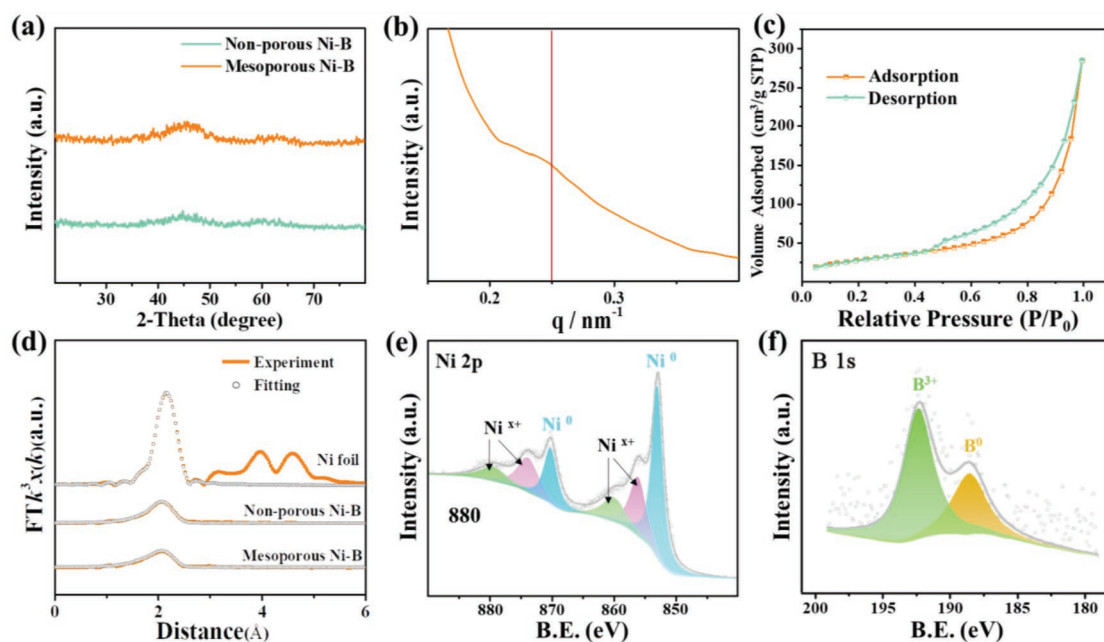
ADVANCED
SCIENCE NEWS
www.advancedsciencenews.com

NANO · MICRO
small
www.small-journal.com

Figure 2. Structural characterization and XPS measurement of the as-prepared samples. a) The wide-angle XRD patterns of mesoporous Ni-B and non-porous Ni-B alloy spheres. b) Small-angle X-ray scattering pattern of mesoporous Ni-B alloy spheres. c) N_2 adsorption–desorption isotherm of the mesoporous Ni-B alloy spheres. d) RDF curves and fitting results of the samples. The XPS spectra e) Ni $2p$ and f) B $1s$ of mesoporous Ni-B alloy spheres.

This difference indicates that a fraction of B enters into the lattice of Ni generating a disordered local structure around the Ni atoms.[42] Figure 2d also shows the curve fit results, which are summarized in **Table 1**. The as-prepared samples have a coordination number of $N_{Ni–Ni} = 4.1$ and $N_{Ni–B} = 3.0$ for mesoporous Ni-B and $N_{Ni–Ni} = 5.5$ and $N_{Ni–B} = 2.2$ for non-porous Ni-B, respectively. The higher $N_{Ni–B}$ of mesoporous Ni-B is likely due to the dispersing effect of surfactants, which enables more B to alloy with the Ni material during the reduction process. Without the micelles, Ni and B atoms tend to segregate into more thermodynamically stable Ni and B phases. The mesoporous and non-porous Ni-B amorphous alloys have shorter Ni-Ni bonding length ($R_0 = 2.44$ Å) than Ni foil (2.48 Å). Both the lower coordination number and shorter Ni-Ni bonding length indicate that Ni active sites in the Ni-B amorphous catalyst are distributed more homogeneously and are highly unsaturated, which facilitates better hydrogen adsorption.[43,44] In X-ray photoelectron spectroscopy (XPS), the Ni $2p$ peaks at a binding energy (BE) of 852.7 eV matches metallic Ni^0 species (Figure 2e,f and Figure S9, Supporting Information).[45] Oxidized Ni is also detected due to the spontaneous oxidation of Ni-B surfaces. However, in
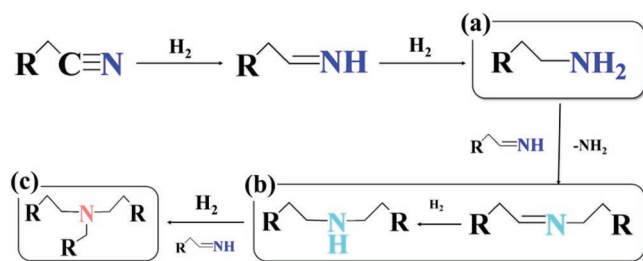
comparison with the pure B (187.1 eV), it is clear that B contained in mesoporous Ni-B is positively shifted by ≈0.8 eV. We attribute this shift to the partial transfer of electrons from B to Ni, while the shift of the Ni peak is not apparent probably because the atomic weight of Ni is much larger than that of B.[23,46] Another explanation is that the electron density around the Ni atom increases due to the electron back-donating effect of B, although this effect does not cause a significant change in the valence state of Ni.[47]

The selective hydrogenation of BC to β-PEA was chosen as the model reaction to assess the activity of mesoporous and non-porous Ni-B alloy catalysts. **Scheme 2** shows the main reaction pathways to primary amines and higher amines. **Figure 3** and Table S2, Supporting Information, show the results obtained with mesoporous and non-porous Ni-B alloy catalysts for the selective hydrogenation of BC to β-PEA. These experiments show that the open 3D mesoporous Ni-B amorphous alloy spheres exhibit a much higher activity and better selectivity for the primary amine versus the non-porous Ni-B alloy spheres. The TOF values are calculated by conversion (<20%) and metal dispersion (Table S2, Supporting Information). The mesoporous

Table 1. The local structural parameters of as-prepared mesoporous Ni-B, non-porous Ni-B, and the Ni foil.

Sample	Shell	N	R_0 [Å]	σ^2 [Å^2]	ΔE_0 [eV]	R factor
Ni foil	Ni-Ni	12	2.48 ± 0.00	0.006	6.8	0.002
Mesoporous Ni-B	Ni-Ni	4.1 ± 0.5	2.44 ± 0.01	0.010	1.2	0.006
	Ni-B	3.0 ± 0.8	2.08 ± 0.01	0.008		
Non-porous Ni-B	Ni-Ni	5.5 ± 0.5	2.44 ± 0.00	0.005	0.6	0.005
	Ni-B	2.2 ± 0.9	2.04 ± 0.02	0.012		

N, coordination numbers; R, bond distance; σ^2, Debye–Waller factors; ΔE_0, the inner potential correction; R factor, goodness of fit.

ADVANCED
SCIENCE NEWS
www.advancedsciencenews.com

NANO · MICRO
small
www.small-journal.com

Scheme 2. Hydrogenation of BC and possible side reactions: a) primary amines, b) secondary amines, and c) tertiary amines.

Ni-B alloy spheres have a much higher intrinsic activity versus the non-porous Ni-B alloy spheres, with TOFs of 11.6 and 3.0 h^{-1}, respectively (Figure 3b). The large 3D pores in the Ni-B spheres may serve as microreactors for the hydrogenation reaction, where multiple reactions can be carried out simultaneously without affecting each other. Moreover, the mesopores in mesoporous Ni-B spheres ensure high dispersion of the Ni active sites (Table S1, Supporting Information), and the large pores may facilitate diffusion and adsorption of reactant molecules.

The H$_2$-TPD curve (Figure 3c) for mesoporous Ni-B amorphous alloy spheres have two main peaks located at 481 and 636 K, whereas non-porous Ni-B amorphous alloy spheres have three peaks located at 441, 571, and 626 K. The lower number of desorption peaks in the mesoporous Ni-B indicates the presence of uniformly distributed active sites. Uniform doping of boron in the mesoporous Ni-B sample enables a better dispersion of Ni atoms and shorter Ni-Ni bond lengths (Table 1), which strengthens the overall cooperativity between the active sites.[48] The high desorption temperature of hydrogen observed in the mesoporous sample is possibly due to the strong synergic effect from neighboring Ni-B. These strongly-adsorbed hydrogen atoms are more active than weakly-adsorbed hydrogen atoms and enable the efficient catalyst surface to hydrogenate a nitro group to an amine.[23] In addition, the mesoporous Ni-B spheres clearly absorb more hydrogen than its non-porous counterpart, according to the hydrogen desorption area in the H$_2$-TPD curves (Figure 3c), which is desirable for boosting the catalytic performance.[49] Furthermore, with the H$_2$ pressure increases from 1 to 5 MPa, the hydrogenation rate of BC gradually increases in a linear manner, exhibiting first-order kinetics with respect to hydrogen (Figure 3d).

As shown in Figure 3b, both mesoporous and non-porous Ni-B samples have a high selectivity for β-PEA, which can be understood by the promoting effect of alloying B, which
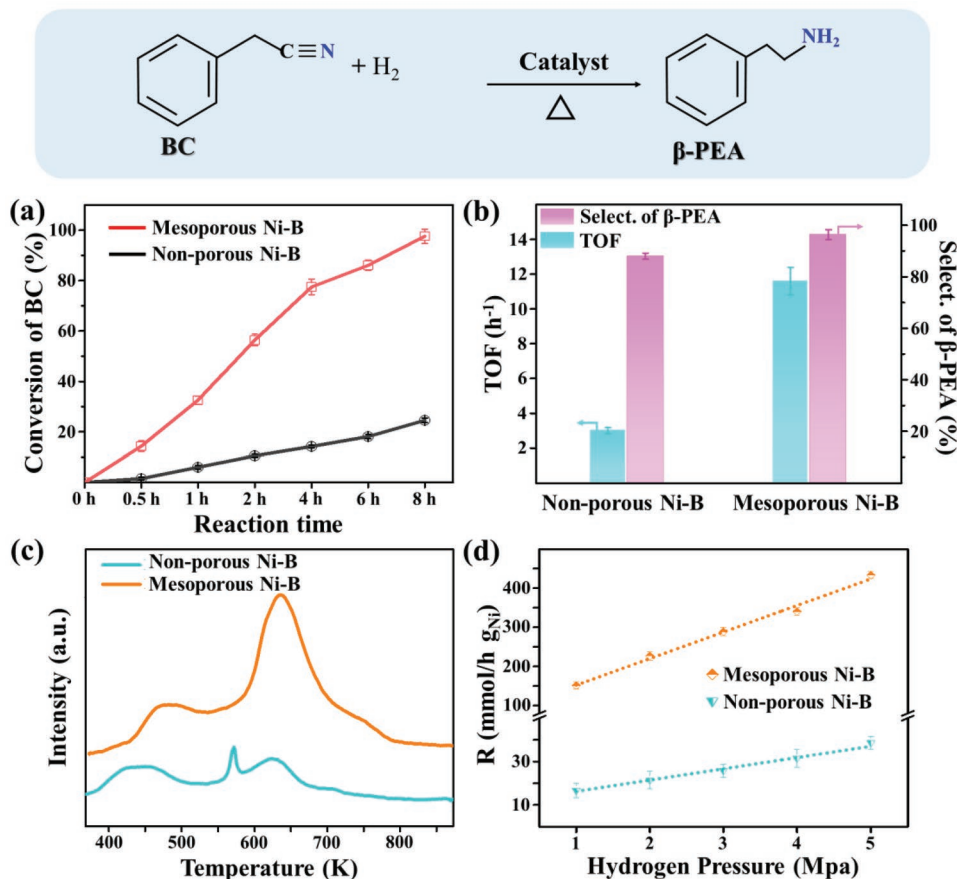

Figure 3. The selective hydrogenation of BC to β-PEA. a) The conversion rates of mesoporous Ni-B and non-porous Ni-B alloy spheres with different reaction times. b) TOF of the two samples obtained at conversion of BC below 20%. c) The H$_2$–TPD curves of the mesoporous Ni-B and non-porous Ni-B alloy spheres. d) Effect of the H$_2$ pressure on the BC hydrogenation rate of both samples. Reaction conditions: 0.08 mmol Ni, 5.0 mmol substrate, 120 °C, 4.0 MPa H$_2$, 20 mL ethanol solution containing 0.5 mL 1,3,5-trimethylbenzene.

**ADVANCED
SCIENCE NEWS**

www.advancedsciencenews.com

**NANO · MICRO
small**

www.small-journal.com

modifies the surface electronic state of Ni, as elaborated in our XPS measurements (Figure 2e,f and Figure S9, Supporting Information). Nitriles may coordinate with transition metals in a linear manner (a so-called end-on fashion) via the lone pairs of the nitrogen (N) atom. However, in most nickel-based catalysts, this dominant end-on fashion quickly poisons the catalyst and makes the carbon atom in C≡N triple bond more prone to a nucleophilic addition reaction, thus reducing selectivity. After alloying with B (as an electron donor), the electron-rich Ni sites tend to repel the lone electron pair of nitrogen atom, inhibiting nucleophilic addition and facilitating a higher selectivity for the primary amine.[50] Thus, the higher selectivity for β-PEA in the mesoporous Ni-B sample may due to the more Ni-B bonds. In addition, our measurements (Figure 2d and Table 1) show that B creates the lower coordination number and shorter Ni-Ni bond lengths, which indicates that Ni active sites are distributed more homogeneously in the material.

3. Conclusion

In summary, we have successfully generated the open 3D mesoporous Ni-B amorphous alloy spheres with high surface areas and a homogenous dispersion of Ni atoms. The synthesis of the mesoporous structure is driven by the self-assembly of structure-directing polymer micelles (PEO-b-PMMA) and dual reducing agents (SBH and DMAB). In the selective hydrogenation of BC to β-PEA, the as-prepared mesoporous Ni-B alloy spheres exhibit excellent intrinsic activity with TOF of 11.6 h^{-1}, nearly four times greater than the non-porous Ni-B alloy spheres (i.e., TOF = 3.0 h^{-1}). The outstanding activity of the catalyst for selective hydrogenation can be attributed to the synergistic effects of the amorphous alloyed Ni-B with the open 3D porous structure, which not only increases surface area but also provides more effective active sites for hydrogen adsorption due to the homogenous dispersity of the Ni and B atoms. This study provides an easy and effective way to prepare mesoporous non-noble metal nanomaterials for heterogeneous hydrogenation reactions. Moreover, the amorphous alloying effects of the catalytic process could be better understood. The details of sample preparation and effective control measures for pores generation will be elaborated in the next part of our work.

4. Experimental Section

Materials: All reagents were used as purchased without further purification. Nickel(II) nitrate hexahydrate (NiCl$_2$·6H$_2$O), dimethylamine borane (DMAB), and sodium borohydride (SBH) were purchased from Sigma Aldrich. The block copolymer, poly(ethylene oxide)-b-methyl methacrylate (PEO$_{10500}$-b-PMMA$_{18000}$) was obtained from Polymer Source. Ethanol and N,N-dimethylformamide (N,N-DMF) were purchased from Adamas-beta. Benzyl cyanide, β-phenylethylamine, and 1,3,5-trimethylbenzene (TB) were purchased from Aladdin Ltd. (Shanghai, China).

Synthesis of the 3D Open Mesoporous Ni–B Amorphous Alloy Spheres: Mesoporous Ni–B alloy spheres were synthesized by self-assembly of micelles by the following steps: 10 mg of PEO$_{10500}$-b-PMMA$_{18000}$ block copolymer was completely dissolved in 0.8 mL of DMF, resulting in a transparent solution. Then, the following solutions were added in this sequence: 0.2 mL of deionized water, 2 mL of

40 mM NiCl$_2$·6H$_2$O, 2 mL of 200 mM DMAB. The formed light green solution was aged for 4 h in a water bath at around 38 °C after a few seconds of ultrasound. After that, a trace amount (0.4 mg) of SBH was used to initiate the reaction. The color of the solution quickly turned black, and the entire reaction completed in 30 min. The samples were collected by centrifugation and washed with acetone several times to remove the template. For comparison, non-porous Ni–B spheres were prepared in the same procedure by omitting the block copolymer.

Characterization: The catalysts' amorphous structure was determined by both XRD (Rigaku D/Max-RB with Cu Kα radiation) and SAED (JEOL JEM-2100). TEM (JEOL-2010F) and SEM (Hitachi SU-4800) were employed to observe particle size and morphology. The surface electronic states were investigated by XPS (ULVAC-PHI PHI5000 VersaProbe using Al Kα radiation), during which all catalyst samples were dried and pretreated in situ in a pure Ar atmosphere to avoid oxidation. The atomic composition of the samples was characterized by inductively coupled plasma optical emission spectroscopy (Varian VISTA-MPX). The dispersion (D) of Ni was calculated from the active surface area which was measured by H$_2$ chemisorption conducted on a Micromeritics-2920 chemisorption apparatus equipped with a thermal conductivity detector. The N$_2$ adsorption–desorption isotherms were obtained at 77 K using a Micromeritics ASAP 2010 instrument in which the specific surface area (S_{BET}) and pore volume (V_P) were calculated by applying BET and Barrett–Joyner–Halenda (BJH) models. The hydrogen temperature-programmed desorption (H$_2$-TPD) curves of as-prepared samples were also obtained by Micromeritics-2920.

Benzyl Cyanide Hydrogenation to β-phenylethylamine: The hydrogenation of BC reaction was performed in a 100 mL high-pressure stainless-steel autoclave, in which the 5 mg catalyst was mixed with 5 mmol substrate, 0.5 mL TB (internal standard) and 20 mL EtOH. After the reactor was purged with H$_2$ and pressurized to 4.0 MP, the system was heated to 120 °C and kept for a specific time under stirring at 1000 rpm. The obtained products were analyzed using a gas chromatograph (Agilent 7890B) equipped with a flame ionization detector (FID) coupled to a 30-meter × 0.320-millimeter DB-624 capillary column. The chromatograms, calculation methods for conversion and selectivity are shown in Figure S10, Supporting Information. The specific activity was calculated using the equation: $n_{BC\ converted}/(n_{metal} \times h)$ where n is moles and h denotes the reaction time. Turnover frequency (TOF) is calculated using the equation: TOF = $n_{BC\ converted} \times M_{Ni}/(D \times W \times h)$, where W is the mass of the catalyst, M_{Ni} is the molar mass of Ni, and D is the dispersion of Ni as determined by H$_2$ chemisorption.

Supporting Information

Supporting Information is available from the Wiley Online Library or from the author.

Conflict of Interest

The authors declare no conflict of interest.

[1] J. C. Ye, J. Lu, C. T. Liu, Q. Wang, Y. Yang, *Nat. Mater.* **2010**, *9*, 619.

[2] M. X. Li, S. F. Zhao, Z. Lu, A. Hirata, P. Wen, H. Y. Bai, M. Chen, J. Schroers, Y. Liu, W. H. Wang, *Nature* **2019**, *569*, 99.

[3] W. E. Brower, M. S. Matyjaszczyk, T. L. Pettit, G. V. Smith, *Nature* **1983**, *301*, 497.

[4] H. Li, H. Yang, H. Li, *J. Catal.* **2007**, *251*, 233.

[5] J. Ma, L. Xu, L. Xu, H. Wang, S. Xu, H. Li, S. Xie, H. Li, *ACS Catal.* **2013**, *3*, 985.

[6] H. Guo, H. Zhang, L. Zhang, C. Wang, F. Peng, Q. Huang, L. Xiong, C. Huang, X. Ouyang, X. Chen, X. Qiu, *Ind. Eng. Chem. Res.* **2018**, *57*, 498.

[7] Y. Pei, G. Zhou, N. Luan, B. Zong, M. Qiao, F. F. Tao, *Chem. Soc. Rev.* **2012**, *41*, 8140.

[8] C. H. Du, Y. Zhao, D. Sun, *Adv. Mater. Res.* **2011**, *183–185*, 2322.

[9] Z. Jiang, H. Yang, Z. Wei, Z. Xie, W. Zhong, S. Wei, *Appl. Catal. A: Gen.* **2005**, *279*, 165.

[10] S. J. Chiang, C.-H. Yang, Y.-Z. Chen, B.-J. Liaw, *Appl. Catal. A: Gen.* **2007**, *326*, 180.

[11] H. Li, Y. Xu, H. Yang, F. Zhang, H. Li, *J. Mol. Catal. A: Chem.* **2009**, *307*, 105.

[12] Y. Xia, N. J. Halas, *MRS Bull.* **2011**, *30*, 338.

[13] S.-J. Zhang, Y.-X. Zheng, L.-S. Yuan, L.-H. Zhao, *J. Power Sources* **2014**, *247*, 428.

[14] Y. Liang, X. Sun, A. M. Asiri, Y. He, *Nanotechnology* **2016**, *27*, 12LT01.

[15] Y. Guo, X. Liu, M. U. Azmat, W. Xu, J. Ren, Y. Wang, G. Lu, *Int. J. Hydrogen Energ.* **2012**, *37*, 227.

[16] J. Shao, X. Xiao, X. Fan, L. Chen, H. Zhu, S. Yu, Z. Gong, S. Li, H. Ge, Q. Wang, *Mater. Lett.* **2013**, *109*, 203.

[17] B. Jiang, H. Song, Y. Kang, S. Wang, Q. Wang, X. Zhou, K. Kani, Y. Guo, J. Ye, H. Li, Y. Sakka, J. Henzie, Y. Yamauchi. *Chem. Sci.* **2020**, *11*, 791.

[18] H. Li, Z. Bian, J. Zhu, D. Zhang, G. Li, Y. Huo, H. Li, Y. Lu, *J. Am. Chem. Soc.* **2007**, *129*, 8406.

[19] H. Li, Z. Bian, J. Zhu, Y. Huo, H. Li, Y. Lu, *J. Am. Chem. Soc.* **2007**, *129*, 4538.

[20] V. Malgras, H. Ataee-Esfahani, H. Wang, B. Jiang, C. Li, K. C. Wu, J. H. Kim, Y. Yamauchi, *Adv. Mater.* **2016**, *28*, 993.

[21] B. Jiang, C. Li, J. Tang, T. Takei, J. H. Kim, Y. Ide, J. Henzie, S. Tominaka, Y. Yamauchi, *Angew. Chem. Int. Ed.* **2016**, *55*, 10037.

[22] B. Jiang, C. Li, O. Dag, H. Abe, T. Takei, T. Imai, M. S. A. Hossain, M. T. Islam, K. Wood, J. Henzie, Y. Yamauchi, *Nat. Commun.* **2017**, *8*, 15581.

[23] H. Li, Q. Zhao, Y. Wan, W. Dai, M. Qiao, *J. Catal.* **2006**, *244*, 251.

[24] H. Li, D. Zhang, G. Li, Y. Xu, Y. Lu, H. Li, *Chem. Commun.* **2010**, *46*, 791.

[25] Y. Yamauchi, T. Momma, T. Yokoshima, K. Kuroda, T. Osaka, *J. Mater. Chem.* **2005**, *15*, 1987.

[26] Y. Yamauchi, T. Yokoshima, H. Mukaibo, M. Tezuka, T. Shigeno, T. Momma, T. Osaka, K. Kuroda, *Chem. Lett.* **2004**, *33*, 542.

[27] O. H. Kim, Y. H. Cho, S. H. Kang, H. Y. Park, M. Kim, J. W. Lim, D. Y. Chung, M. J. Lee, H. Choe, Y. E. Sung, *Nat. Commun.* **2013**, *4*, 2473.

[28] J. Wei, Z. Sun, W. Luo, Y. Li, A. A. Elzatahry, A. M. Al-Enizi, Y. Deng, D. Zhao, *J. Am. Chem. Soc.* **2017**, *139*, 1706.

[29] J. Tang, J. Liu, C. Li, Y. Li, M. O. Tade, S. Dai, Y. Yamauchi, *Angew. Chem. Int. Ed.* **2015**, *54*, 588.

[30] D. B. Bagal, B. M. Bhanage, *Adv. Synth. Catal.* **2015**, *357*, 883.

[31] K. Tokmic, B. J. Jackson, A. Salazar, T. J. Woods, A. R. Fout, *J. Am. Chem. Soc.* **2017**, *139*, 13554.

[32] Z. Shao, S. Fu, M. Wei, S. Zhou, Q. Liu, *Angew. Chem. Int. Ed.* **2016**, *55*, 14653.

[33] M. Vilches-Herrera, S. Werkmeister, K. Junge, A. Börner, M. Beller, *Catal. Sci. Technol.* **2014**, *4*, 629.

[34] A. Mukherjee, D. Srimani, S. Chakraborty, Y. Ben-David, D. Milstein, *J. Am. Chem. Soc.* **2015**, *137*, 8888.

[35] M. R. Libera, R. F. Egerton, *Polym. Rev.* **2010**, *50*, 321.

[36] J. P. Patterson, M. P. Robin, C. Chassenieux, O. Colombani, R. K. O'Reilly, *Chem. Soc. Rev.* **2014**, *43*, 2412.

[37] D. He, L. Zhang, D. He, G. Zhou, Y. Lin, Z. Deng, X. Hong, Y. Wu, C. Chen, Y. Li, *Nat. Commun.* **2016**, *7*, 12362.

[38] S. Wei, H. Oyanagi, Z. Li, X. Zhang, W. Liu, S. Yin, X. Wang, *Phys. Rev. A* **2001**, *63*, 224201.

[39] Y. Lu, H. Fan, A. Stump, T. L. Ward, T. Rieker, C. J. Brinker, *Nature* **1999**, *398*, 223.

[40] E. Daryl Crozier, *Physica. B* **1995**, *208–209*, 330.

[41] H. Li, H. Li, J.-F. Deng, *Appl. Catal. A: Gen.* **2000**, *193*, 9.

[42] Z. Wei, Z. Li, Z. Jiang, J. Ye, W. Zhong, J. Song, S. Wei, *J. Alloy. Comp.* **2008**, *460*, 553.

[43] H. Li, H. Li, J.-F. Deng, *Catal. Today* **2002**, *74*, 53.

[44] B. Shen, S. Wei, K. Fang, J.-F. Deng, *Appl. Phys. A* **1997**, *65*, 295.

[45] H. Wang, K. Xu, X. Yao, D. Ye, Y. Pei, H. Hu, M. Qiao, Z. H. Li, X. Zhang, B. Zong, *ACS Catal.* **2018**, *8*, 1207.

[46] Y. Hou, Y. Wang, Z. Mi, *J. Mater. Sci.* **2005**, *40*, 6585.

[47] S. Carenco, D. Portehault, C. Boissiere, N. Mezailles, C. Sanchez, *Chem. Rev.* **2013**, *113*, 7981.

[48] J.-F. Deng, H. Li, W. Wang, *Catal. Today* **1999**, *51*, 113.

[49] H. Li, W. Wang, H. Li, J.-F. Deng, *J. Catal.* **2000**, *194*, 211.

[50] S. Xie, H. Li, H. Li, J.-F. Deng, *Appl. Catal. A: Gen.* **1999**, *189*, 45.